energies

Article

A Comprehensive Study on the Hydrogeochemical and Isotope Characteristics and Genetic Mechanism of Geothermal Water in the Northern Jinan Region

Zongjun Gao, Mengyuan Hao, Jiutan Liu *, Qiang Li, Menghan Tan and Yiru Niu

College Of Earth Science and Engineering, Shandong University of Science and Technology, Qingdao 266590, China; gaozongjun@sdust.edu.cn (Z.G.); hmysdust@126.com (M.H.); qiangli6110@126.com (Q.L.); tmhsdust@126.com (M.T.); nyrsdkj@126.com (Y.N.)
* Correspondence: ljtsdust@sdust.edu.cn

Abstract: Geothermal water (GW) resources are highly valued as clean, renewable energy sources. In this study, a comprehensive analysis of water chemistry and isotope data from 25 GW samples was conducted to gain insights into the hydrochemical characteristics and formation mechanisms of the GW in the northern Jinan region (NJR). Statistical analysis and hydrochemical methods were employed for relevant analysis. The findings reveal that the GW in the NJR exhibits high salinity, with an average total dissolved solids (TDS) concentration of 9009.00 mg/L. The major ions identified are Na^+ and Cl^-, with mean concentrations of 2829.73 mg/L and 4425.77 mg/L, respectively, resulting in a hydrochemical type of Cl^-Na. The analysis of δ^2H and $\delta^{18}O$ isotopes indicates that the GW originates from atmospheric precipitation that undergoes deep cycling and interaction with older groundwater. The composition of ^3H suggests that the GW in the NJR is a mixture of waters, while radiocarbon dating (^{14}C) suggests that the recharge of the GW may have occurred in the late Pleistocene era. The GW in the NJR is classified as partially equilibrated waters. The temperature range of geothermal reservoirs is 57.13 to 99.74 °C. The hydrochemical components primarily result from water–rock interactions, including silicate weathering, cation exchange, as well as carbonate weathering and the dissolution of halite and gypsum. Moreover, taking into account the hydrogeological conditions, hydrochemistry, and isotope analysis, a conceptual model of the geothermal reservoir in the NJR was developed. The research findings serve as a valuable reference and foundation for the development and utilization of geothermal resources in the Jinan region. These originate from the Taiyi mountains in the south or the Taihang mountains in the west, and experience deep circulation and long runoff times. This study provides a reference for the sustainable development and utilization of regional geothermal resources.

Keywords: hydrochemical characteristics; isotope composition; genetic mechanism; GW; northern Jinan region

Citation: Gao, Z.; Hao, M.; Liu, J.; Li, Q.; Tan, M.; Niu, Y. A Comprehensive Study on the Hydrogeochemical and Isotope Characteristics and Genetic Mechanism of Geothermal Water in the Northern Jinan Region. *Energies* **2023**, *16*, 7658. https://doi.org/10.3390/en16227658

Academic Editors: Benjamin McLellan and Rafael Santos

Received: 26 September 2023
Revised: 13 November 2023
Accepted: 14 November 2023
Published: 19 November 2023

1. Introduction

Geothermal energy is a significant natural resource found within the Earth's interior [1]. Global statistics from 2015 to 2019 indicate that a total of 2647 geothermal wells were utilized over that period for geothermal power generation or direct heating in 42 countries [2]. Furthermore, the installed capacity for direct utilization of geothermal resources worldwide in 2019 reached 1.07×10^6 MWt. In China, the available geothermal resources account for nearly 8% of the global total, representing substantial development potential [3,4]. However, despite this potential, the development and utilization of geothermal resources in China has lagged behind wind and solar energy, primarily due to a lack of comprehensive industrial planning, policy support, and outdated mining techniques [3].

Geothermal fluid serves as the primary medium for the development and utilization of geothermal resources, possessing dual attributes as both water resources and mineral resources. It represents a clean and environmentally friendly source of energy, harboring significant potential for development and utilization [5]. High-temperature GW can be harnessed for power generation, while medium-to-low-temperature GW finds application in heating, bathing, medical care, and other sectors, thus fostering the growth of associated industries [5].

The chemical composition and origin of GW are typically linked to the intricate geological processes and specific hydrogeochemical conditions within a given region [6]. Investigating the hydrochemical characteristics of GW provides insights into the source, origin, age, migration, storage state, reservoir temperature, and other properties of the geothermal fluid. It also enables the examination of information pertaining to geothermal geological conditions through water–rock interactions [7–10]. Currently, statistical methods [5,11], hydrochemical graphing techniques [12,13], and environmental isotope analyses [13,14] are widely employed, offering valuable insights into the formation mechanisms of GW.

Jinan stands as a renowned “spring city” globally, boasting abundant geothermal resources and promising prospects for development and utilization [15]. Previous investigations on geothermal resources in the northern Jinan region (NJR) have primarily concentrated on the region’s geothermal geological characteristics, recharge sources, and circulation patterns, yielding fruitful research results [14,16–19]. These studies highlight the way that the formation of GW in NJR is influenced by geological structures and magmatic activities. The primary recharge source for GW emerges from atmospheric precipitation in the mountainous areas of southern Jinan, facilitated by deep runoff. Moreover, carbonate and sulfate mineral dissolution, as well as halite precipitation, play crucial roles in governing the hydrochemical characteristics of groundwater. Precipitation from the southern mountains seeps downward into the ground and is then blocked by the Jejunum intrusive rocks and can only progress downward to greater depths, where the groundwater is heated by a geothermal gradient. The heated water eventually reaches the north and forms GW. The depth of the low-velocity layer under the Jinan intrusive rocks varies with the lateral direction, which may indicate that the depth of groundwater transport under the west and east Jinan intrusive rocks is different. Isotopic data have allowed the origin of thermal water to be determined and have presented different recharge elevations. Reservoir temperature was estimated by chemical geothermometry and validated by fluid–mineral equilibria calculations. The feasibility of different geothermometers was verified, indicating that quartz geothermometers were more suitable for the geothermal system [14,20]. However, the majority of these studies mainly focused on the southern section of the Qihe–Guangrao fault in NJR, limiting geothermal research in the northern segment of this fault. The cationic and SiO_2 geothermometers indicate the heat storage temperature in the NJR. The main hydrogeochemical processes of the chemical composition of GWr in the north of Jinan were analyzed by ion ratio. The use of PHREEQC3.1.1 software indicates that GW in the north of Jinan is partially balanced. A conceptual model of geothermal genesis in the northern area of Jinan was established in order to provide conditions for its subsequent rational development and utilization.

Previous studies have focused on the geothermal geologic features, recharge sources and circulation patterns in the southern part of the Qihe–Guangrao rupture, as does this study. Hence, considering the geothermal geological conditions in the NJR, this research employs a comprehensive approach combining hydrochemical and isotopic methods to investigate the hydrochemical characteristics and formation mechanisms of GW. The purpose of this paper is to provide theoretical support for the hydrogeochemical isotope characterization and genesis mechanism of GW in the northern part of the country, and to provide a scientific basis for the development of GW in the northern part of the country.

2. Study Area

The NJR (Figure 1a) is situated in the northern part of Jinan city, to the north of the Qihe–Guangrao fault (Figure 1b). It encompasses Shanghe county, the northern part of

Jiyang county, and the northwestern part of Zhangqiu city. The geographical coordinates span from 116°52′00″ E to 117°27′00″ E and 36°57′00″ N to 37°32′00″ N, covering a total area of 1989 km^2. The terrain in NJR generally exhibits higher elevation in the southwest and lower elevation in the northeast. The northern yellow floodplain area typically features elevations ranging from 10 to 30 m, with a terrain slope of approximately 0.03‰. The lowest point is located in the northeastern part of Shanghe county, with an elevation of 10.7 m. The landform is primarily characterized by Quaternary alluvial plains, resulting in relatively simple terrain. The topography is predominantly a gently sloping low plain, with some areas transitioning into piedmont sloping plains.

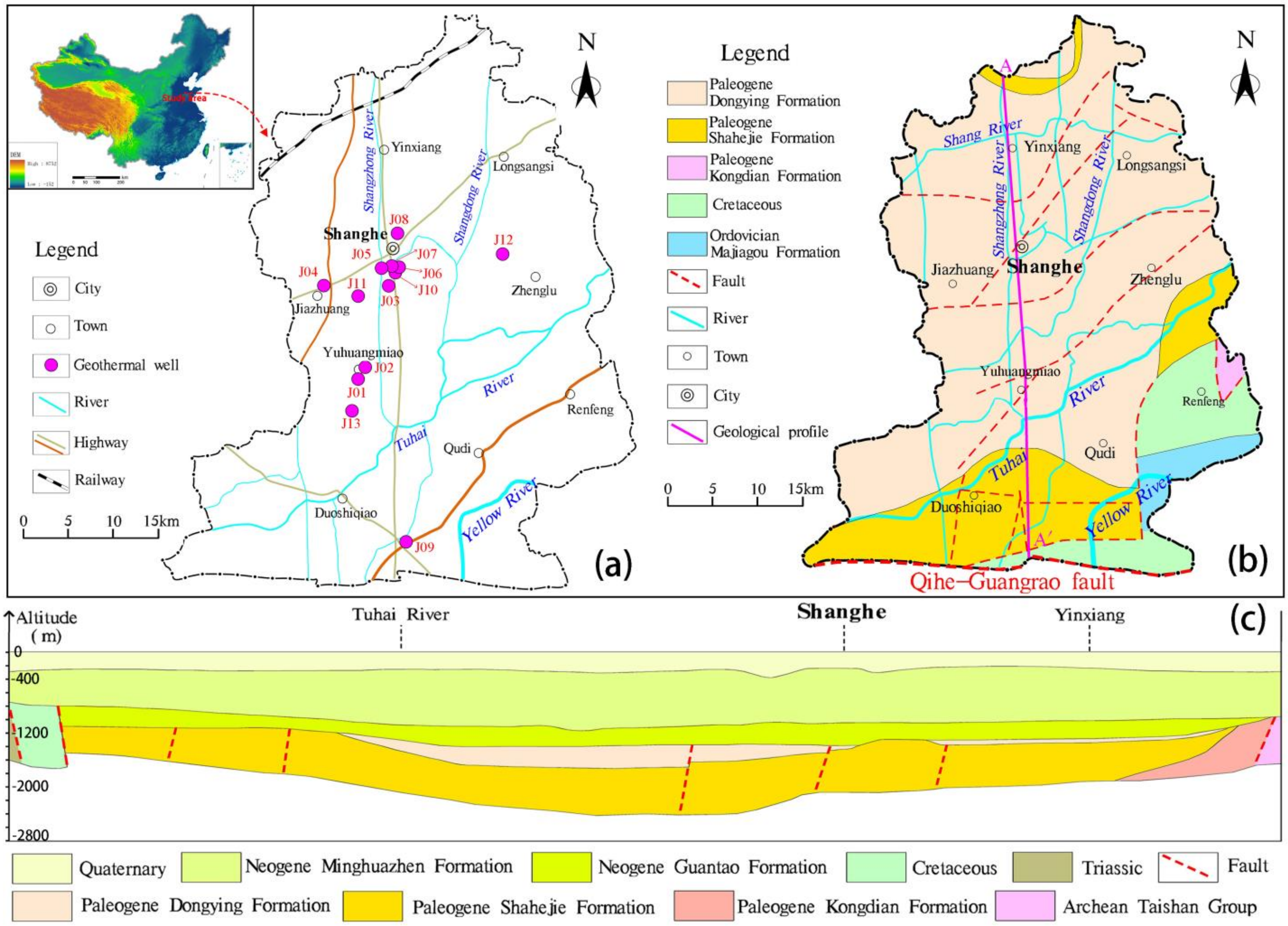

Figure 1. Map of Location and distribution of geothermal wells (**a**), pre-Neogene geological (**b**) and geological cross section (**c**).

The NJR experiences a warm temperate continental climate. It is characterized by dry and less rainy springs, hot and rainy summers, cool and breezy autumns, and severely cold and dry winters. The annual average temperature in the region is 13.6 °C (1956 to 2015), and the average annual precipitation amounts to 614.0 mm. More than 70% of the total precipitation is concentrated in the months of July to September, while the period from December to March of the following year witnesses comparatively less rainfall. The NJR falls within the water system areas of both the Yellow River and Tuhai River. Within the Tuhai River water system area, most of the rivers flow in a southwest to northeast direction; the south side of the Tuhai River, however, flows in a southeast to northwest direction before joining the Tuhai River.

In the NJR, the geological formations are arranged in a top-to-bottom sequence, including the Quaternary, Neogene Minghuazhen Formation, Guantao Formation, Paleogene Dongying Formation, Shahejie Formation, Kongdian Formation, and Cretaceous. Among these formations, the Neogene Guantao Formation and the Paleogene Dongying Formation are widely distributed and characterized by substantial thickness. The Cambrian–Ordovician formations, on the other hand, are deeply buried. The primary type of groundwater in the NJR is pore water, which occurs in the upper loose sediments of the Quaternary and Neogene Minghuazhen Formation. The recharge of groundwater is mainly influenced by atmospheric precipitation and infiltration from rivers, both of which are significant sources of groundwater replenishment.

3. Materials and Methods

3.1. Sampling

In this study, a total of 25 GW samples were collected from 13 geothermal wells in NJR (Figure 1). The geothermal wells were sampled at different frequencies: J02 and J04 were sampled three and four times, respectively, spanning different years. J11, J12, J09, and J01 were sampled once, while the remaining geothermal wells were sampled twice, across different years. All water samples underwent hydrochemical analysis, with eight samples also being tested for hydrogen and oxygen isotopes (δ^2H and $\delta^{18}O$) as well as tritium (^3H) isotopes. Additionally, five water samples were subjected to radiocarbon (^{14}C) isotope testing. The locations of the geothermal wells are indicated in Figure 1, and their depths range from 1300 to 2000 m. Temperature measurements were conducted using a deep well detector (SYKJ-6), comprising various components such as the host, measuring line, electronic point thermometer, depth sensor, and display. The temperature measurement range spanned from 0 to 500 m, with a resolution capability of 0.1 °C and an accuracy of ±0.5%.

To collect GW samples for the main chemical component test, a 5 L rigid polyethylene plastic bucket was utilized. Prior to sampling, it is recommended to clean the sampling barrel 2–3 times using the GW that will be collected. It is important to fill these bottles without introducing any bubbles, and seal them tightly using parafilm for storage. Once the sampling is completed, it is advisable to send the samples to the laboratory for testing as soon as possible.

3.2. Analysis Method

The pH of the GW sample was measured using a pH meter (China Shanghai Yidian Scientific Instrument Co., Shanghai, China, PHS-3C). The levels of total hardness (TH), total dissolved solids (TDS), K^+, Na^+, Ca^{2+}, Mg^{2+}, and H_3SiO_3 were determined using an inductively coupled plasma emission spectrometer (ICP, PerkinElmer Corporation, Waltham, MA, USA, Optima 7000DV). The concentrations of $SO_4{}^{2-}$, Cl^-, and $NO_3{}^-$ were tested using an ion chromatograph (Thermo Fisher Scientific Co., Waltham, MA, USA, ICS-600), while $HCO_3{}^-$ was determined through titration. Stable isotope analysis of δ^2H and $\delta^{18}O$ was conducted using a stable isotope mass spectrometer (Thermo Fisher Scientific Co., MAT-253), while measurements of 3H and ^{14}C were performed using an ultra-low background liquid scintillation spectrometer (Revvity Co., Waltham, MA, USA, Quantulus-220).

The Piper diagram was used to determine the type of water chemistry and analyze geothermal water chemistry, Schoeller diagrams were used to characterize water chemistry, and Na-K-Mg triangles were used to assess water–rock equilibrium and to differentiate between water samples. Gibbers plots were used to determine the primary mechanism controlling water chemistry, ion ratio plots to determine the source of water chemistry, and saturation indices (SI) to determine mineral dissolution or precipitation. SI was calculated using the PHREEQC software based on the mathematical relationship between the ionic activity product and the corresponding equilibrium constant.

4. Results and Discussions

4.1. Hydrochemical Characteristics of GW

Descriptive statistical analysis proves beneficial in comprehending the general characteristics, enrichment, and variation exhibited by various chemical components present in GW. Table 1 presents the statistical findings concerning the primary physical and chemical components found in GW of NJR. GW temperature falls within the range of 54 °C and 59 °C, with an average of 56.75 °C. The pH values span between 7.15 and 7.55, averaging at 7.42, thereby indicating the weak alkaline nature of the GW in the NJR. TDS concentration in the NJR is relatively high, ranging from 5568.20 mg/L to 12,156.00 mg/L, with an average concentration of 9009.00 mg/L. Dominant cations and anions in GW are Na^+ and Cl^-, respectively, with concentrations ranging from 1755.00–3755.00 mg/L and 2445.30–6649.00 mg/L. The average values for Na^+ and Cl^- are 2829.73 mg/L and 4425.77 mg/L, respectively. Regarding cationic presence, the order is $Na^+ > Ca^{2+} > Mg^{2+} > K^+$. Anionic composition exhibits a hierarchy of $Cl^- > SO_4^{2-} > HCO_3^- > NO_3^-$. Specific data are detailed in Table S1 of the Supplementary Material.

Table 1. Statistical characteristics of the main chemical components of GW.

	Units	Max	Min	Mean	SD
K^+	mg/L	67.3	3.7	23.0	13.0
Na^+	mg/L	3775.0	1755.0	2829.7	548.3
Ca^{2+}	mg/L	650.4	169.8	401.7	153.9
Mg^{2+}	mg/L	117.6	36.5	78.5	25.6
Cl^-	mg/L	6649.0	2445.3	4425.8	1338.1
SO_4^{2-}	mg/L	2903.4	280.5	1067.8	468.4
HCO_3^-	mg/L	231.1	26.2	155.8	53.7
NO_3^-	mg/L	5.9	0.02	1.6	1.5
TH	mg/L	2087.0	603.12	1308.3	479.2
TDS	mg/L	12,156.0	5568.2	9009.0	1755.3
pH	/	7.7	7.1	7.4	0.16
SiO_2	mg/L	29.0	22.6	26.3	1.3
Temperature	°C	59.0	54.0	56.8	1.2
δ^2H	‰	−69.1	−76.0	−72.2	2.6
$\delta^{18}O$	‰	−8.0	−9.3	−8.8	0.5
^3H	TU	20.6 ± 1.0	2.7 ± 0.1	/	/
^{14}C age	ka BP	13.4 ± 0.5	1.0 ± 0.1	/	/

The utilization of the Piper diagram [21] for analyzing water chemistry characteristics is widely employed and serves as a straightforward and efficient tool for hydrochemical classification [22]. As depicted in Figure 2, the GW samples predominantly cluster within the [Cl^-] and [Na^+] regions of the anion and cation triangle beneath the Piper diagram. Upon projection onto the upper diamond, the water sample points fall within area ②, indicating that the hydrochemical type of deep GW in northern Jinan is uniformly classified as Cl^-Na type.

4.2. Isotopic Composition Characteristics

δ2 H/δ^{18}O and 3H/14C

Isotope methods play a crucial role in determining groundwater origin, recharge elevation, and hydraulic connections between different water bodies [14,19]. In Table 1, the δ2H and δ18O values of the GW in the NJR ranged from −69.96 to −75.98 and −7.94 to −9.25, with mean values of −72.61 and −8.72, respectively. Figure 3 illustrates the relationship between δ2H-δ18O in the GW of NJR. The global meteoric water line (GWML) and the local meteoric water line (LWML) in Figure 3 are derived from previous studies conducted by Craig [23] and Liu et al. [24]. As is evident from Figure 3, the GW sample points can be roughly divided into two groups, namely group (I) and group (II). The water samples in group (I) are closely clustered around the LWML, indicating that they are derived from direct or indirect precipitation in the atmosphere. Due to the influence of the Qihe–Guangrao fault, the depth of groundwater infiltration increases, and the gradually increasing temperature and pressure inside the stratum force the oxygen isotope of the infiltrated atmospheric precipitation to evaporate, or to react with the surrounding rock, and the oxygen isotope exchange of water and minerals, resulting in the oxygen isotope in the GW. Drift, and then the earth's heat flow through the deep circulation forms GW. The extent of this drift depends on factors such as water/rock ratio, interaction strength, and reaction time frame. The water samples belonging to group (II) deviate from the LWML distribution to the right, indicating obvious oxygen isotope drift. This indicates that the NJR GW is less affected by faulting and may originate from older water sources. The water–rock isotope exchange is clear and the cycle period is long. The isotope 3H, a radioactive isotope of hydrogen, serves as a valuable dating technique in hydrogeological research, providing radiometric timing [19,25]. Groundwater typically experiences minimal exchange with surrounding rock media, allowing the 3H content to be solely governed by radioactive decay. As such, it proves useful in investigating hydrogeological and geothermal development issues. When the 3H content is less than 0.8TU, this indicates that the groundwater age is older, and that its source is mainly atmospheric precipitation or formation water before 1950. The range of 0.8–4 TU indicates that atmospheric precipitation after 1950 infiltrated into groundwater, forming a mixture of modern atmospheric precipitation and ancient precipitation or formation water, while the range of 5–15 TU indicates that groundwater is recharged by modern atmospheric precipitation infiltration [26]. In this study, the 3H content is between 2.7~20.6 TU (Table 1), but is slightly biased to 4 TU, indicating that the GW in the NJR is a mixture of modern infiltration water and groundwater or formation water before 1950. Combined with the results of deuterium and oxygen isotope analysis, it can be seen that the GW in the NJR is a mixture of modern infiltration water and formation water before 1950.

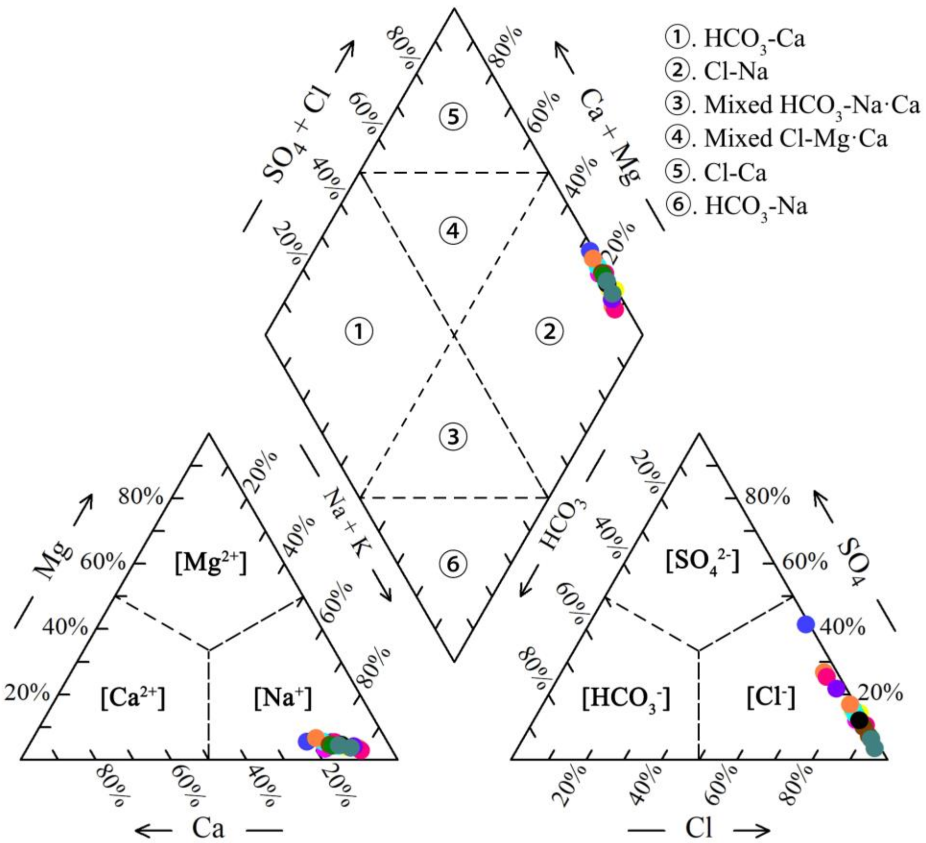

Figure 2. Piper diagram of GW sample in NJR.

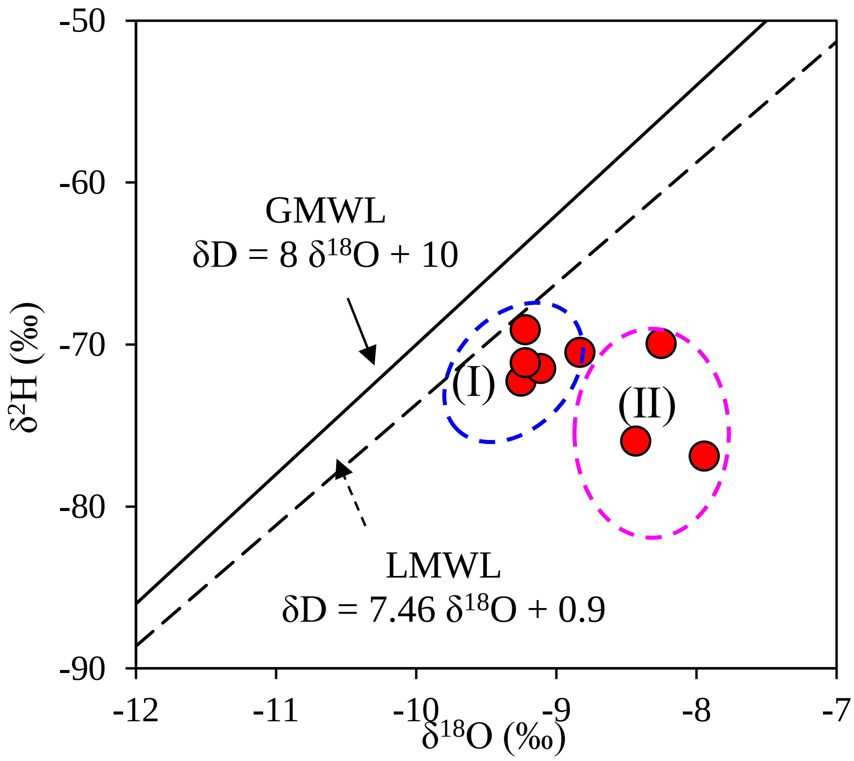

Figure 3. Relationship between δD−δ^{18}O in deep GW in NJR.

The 14C dating method is a well-established technique for dating old groundwater and GW and is particularly suited for measuring ages within the range of 100–50,000 years BP [14]. The 14C ages of the GW in the NJR range from 13.36 to 3.85 ka BP (Table 1), suggesting that recharge may have occurred during the late Pleistocene period. Determination of the age of geothermal water provides a reliable analytical basis for later production capacity evaluation, heat preservation and transportation, groundwater recharge, production capacity optimization, intelligent exploitation, and comprehensive utilization.

4.3. Geothermal Reservoir Temperature

Geothermometers serve as a valuable tool in estimating the temperature of geothermal reservoirs. They utilize the relationship between chemical components, isotope values, and temperature in GW. Geothermometers find widespread application in studying the formation mechanisms, predicting the potential, and exploring and developing geothermal resources [14,25]. Typically, four types of geothermometers are utilized: cation geothermometers, SiO_2 geothermometers, gas geothermometers, and isotope geothermometers. Each type has its specific application conditions [27]. The above hydrochemical characteristics show that the chemical type of NJR GW is dominated by Na-Cl type water with a high content of Na^+, and analysis of the isotopes shows that there is a high amount of silica in the NJR GW, therefore, when estimating the reservoir temperature of GW samples in NJR, cation and silicon chemical geothermometers were employed. The SiO_2 geothermal temperature scale was chosen because the abundance of silicon is sufficient and does not change after equilibration. The relationship between cation exchange and temperature can be confirmed in the study area, so a cation temperature scale was also used. The calculated statistical results are presented in Table 2.

Table 2. Statistical results of estimating reservoir temperature using the selected chemical geothermometer.

		Maximum	Minimum	Mean	Standard Deviation	
(°C)	Quartz	99.74	70.21	92.67	6.56	[26]
(°C)	Quartz (maximum steam loss)	81.83	57.13	75.94	5.47	[26]
(°C)	Chalcedony	46.59	17.69	39.62	6.42	[26]
(°C)	Chalcedony (maximum steam loss)	49.39	21.95	42.79	6.09	[28]
(°C)	Na-K-Mg	−223.03	−236.11	−229.57	2.83	[29]
(°C)	Na-K-Ca-Mg	152.53	117.09	141.34	9.51	[28]
(°C)	Na-K	96.08	18.04	32.81	26.89	[29]
(°C)	K-Mg	86.53	51.43	64.57	14.33	[30]
(°C)	Na-K-Ca	187.29	63.93	129.26	26.99	[31]

Generally, a higher concentration of silica in GW correlates with a higher thermal reservoir temperature [25]. However, it is worth noting that the temperature estimated by the silica geothermometer tends to be higher than the measured temperature of the GW. This discrepancy suggests that other factors may be influencing the temperature estimation process. Additionally, the calculated temperatures from the chalcedony geothermometer are lower than both the measured temperatures and the temperatures obtained from quartz geothermometers. This indicates that the chalcedony geothermometer may not be suitable for accurately estimating the temperature of the geothermal reservoir in the NJR. Therefore, the lowest value of the quartz (maximum vapor loss) calculation and the highest value of the quartz calculation were chosen for the thermal storage temperature range.

Silica geothermometers provide temperature estimations based on different silica mineral phases. The calculated temperature ranges for quartz and quartz with maximum steam loss are 70.21 to 99.74 °C and 57.13 to 81.83 °C, with mean values of 92.67 °C and 75.94 °C, respectively. For chalcedony and chalcedony with maximum steam loss, the calculated temperature ranges are 17.69 to 46.59 °C and 21.95 to 49.39 °C, with average values of 39.62 °C and 42.79 °C, respectively. Furthermore, the temperatures obtained using different cation geothermometers are as follows: (1) the calculated temperatures from the Na-K-Mg geothermometer range from −223.03 °C to −236.11 °C, with an average of −229.57 °C; (2) the Na-K-Ca-Mg geothermometer yields temperatures ranging from 117.09 °C to 152.53 °C, with an average of 141.34 °C; (3) the Na-K geothermometer provides temperatures ranging from 18.04 °C to 96.08 °C, with an average of 32.81 °C; (4) the calculated temperature range of the K-Mg geothermometer is 51.43 °C to 86.53 °C, with an average of 64.57 °C; and (5) the Na-K-Ca geothermometer calculates temperatures ranging from 63.93 °C to 187.29 °C, with an average of 129.26 °C. In general, when the reservoir temperature exceeds 150 °C, it is appropriate to utilize the Na-K geothermometer method to estimate the temperature [25]. This method relies on the sodium-to-potassium ratio controlled by minerals such as albite and potassium feldspar present in the geothermal system. However, as shown in Table 2, the estimated temperature range provided by the Na-K geothermometer is relatively large, and some water samples yield temperatures significantly lower than the measured temperature. This suggests that the Na-K geothermometer may not accurately estimate the temperature in all cases. Furthermore, it is worth noting that the calculated temperatures from the Na-K-Mg geothermometer are anomalously lower compared with the measured temperatures (Table 1). This indicates that the Na-K-Mg geothermometer is not suitable for accurately estimating the temperature of the geothermal reservoir.

The Na-K-Mg triangle diagram, proposed by Giggenbach [32] in 1988, serves as a tool to assess the water–rock balance state and to differentiate the various types of water samples. It classifies water samples into three states or types: complete balance, partial balance, mixed waters, and immature water. As depicted in Figure 4, all of the GW samples in the NJR fall within the zone of partially mature and mixed waters. This suggests that water–rock interaction plays a crucial role in shaping the chemical composition of GW. However, it also indicates that the fluid and minerals have not yet reached a state of complete chemical equilibrium. Furthermore, in the NJR, the composition of GW is influenced by the mixing and dilution processes involving groundwater from different recharge sources. This indicates that the GW in the region undergoes interactions with various water sources, resulting in a complex mixture.

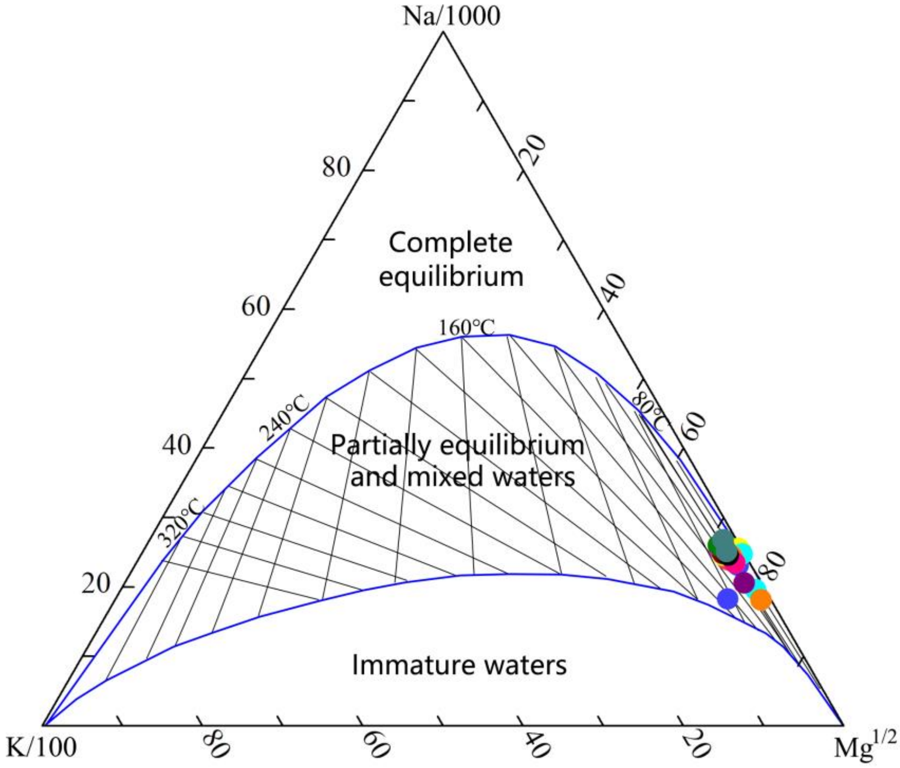

Figure 4. Na-K-Mg Giggenbach diagram with GW samples in NJR.

4.4. Controlling Factors of Hydrochemical Characteristics of GW

4.4.1. Schoeller Diagram

The Schoeller diagram, depicted in Figure 5, is extensively utilized in the analysis of water chemistry characteristics. It effectively illustrates fluctuations in the concentration of major ions present in water samples [5,33,34]. When water samples of the same hydrochemical type display parallel lines connecting two ions, it signifies a consistent or similar concentration ratio between those ions. Conversely, if the ion concentrations of two water samples differ, with one positioned above the other on the diagram, it indicates the relative movement direction of groundwater chemical components across different sampling points. This implies a flow of water from regions of lower concentration to those of higher concentration. SO_4^{2-} and HCO_3^- fluctuated greatly, and the other elements fluctuated more consistently (Figure 5). Furthermore, the variation trends observed in the 25 GW samples collected within the NJR can be broadly classified into two groups, consistent with the findings from the δ2H and δ18O analysis. This suggests potential disparities in the recharge sources of GW.

4.4.2. Correlation Analysis

Correlation analysis is commonly employed to investigate the origins of ions, with components from the same source typically displaying notable correlations. Figure 6 depicts the correlation matrix diagram of the principal chemical components found in the GW of northern Jinan. Notably, TDS exhibits a strong correlation with Cl^- (r = 0.95), Na^+ (r = 0.95), Ca^{2+} (r = 0.86), and Mg^{2+} (r = 0.84), indicating that these chemical components make significant contributions to TDS. Additionally, Ca^{2+} shows a strong correlation with Na^+ (r = 0.95) and K^+ (r = 0.54), suggesting a potential common source, likely originating from the dissolution of silicate minerals. Furthermore, a significant correlation exists between

Ca^{2+} and Mg^{2+} (r = 0.89), indicating that the dissolution of carbonate rock minerals may serve as a significant source of Ca^{2+} and Mg^{2+} in GW.

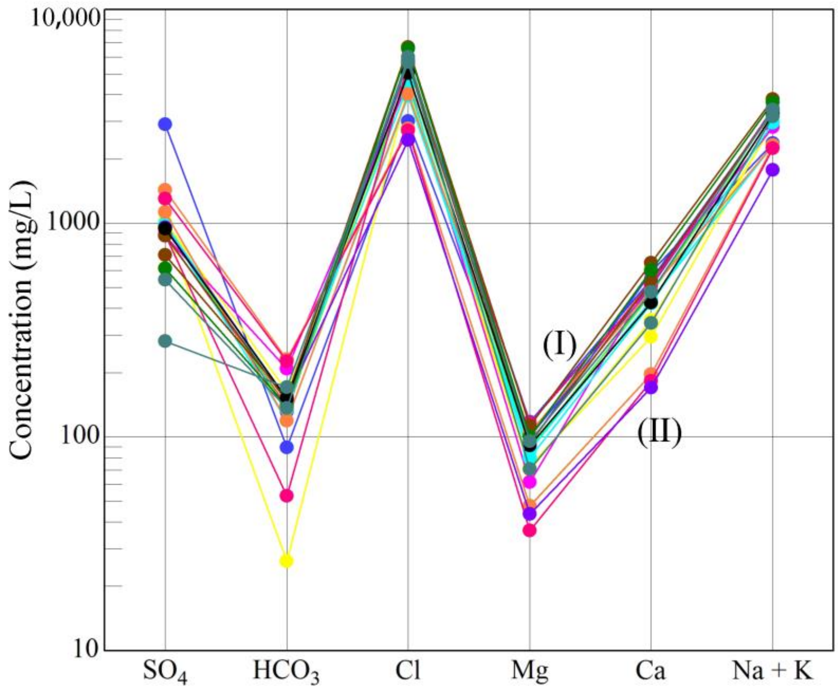

Figure 5. Schoeller diagram of GW samples.

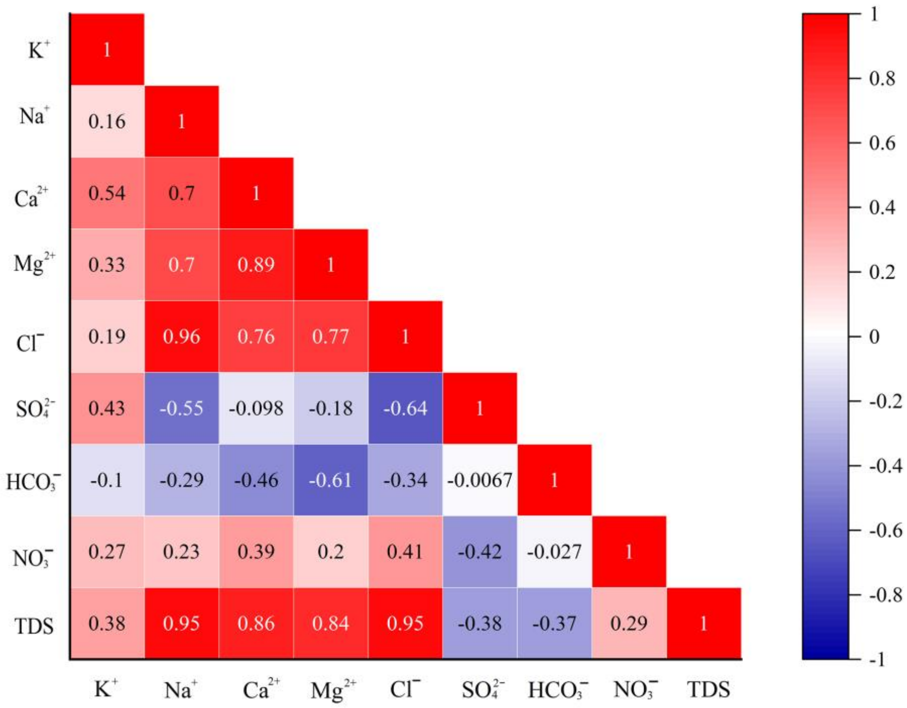

Figure 6. Correlation matrix of GW in northern Jinan.

Cl^- is widely considered a conservative parameter and plays a crucial role in analyzing the chemical characteristics of GW due to the limited presence of chlorine-containing minerals in aquifers, apart from halite [5,35,36]. It exhibits a positive correlation with Na^+ (r = 0.96), Ca^{2+} (r = 0.76), and Mg^{2+} (r = 0.77), while showing a negative correlation with SO_4^{2-} (r = −0.64) and HCO_3^- (r = 0.34). Throughout the protracted flow process of

GW, leaching, evaporation, and concentration occur, leading to an increase in Cl^- content and a decrease in HCO_3^- and SO_4^{2-} content. Additionally, the ratios of HCO_3^-/Cl^- (0.006~0.008) and SO_4^{2-}/Cl^- (0.05~0.97) in GW are relatively low, indicating an extended runoff path and a slower deep-water cycle for GW [35].

4.4.3. Ion Ratios Analysis

Typically, the chemical composition of water is influenced by various factors, such as rock weathering, atmospheric precipitation, and evaporation [37]. However, GW follows an extensive circulation path and undergoes continuous leaching, evaporation, and concentration, resulting in a high salinity level. Consequently, evaporation becomes the primary controlling factor for the chemical characteristics of GW. This is further illustrated by the distribution of GW samples in the Gibbs diagram [37] (Figure 7), emphasizing the dominance of evaporation in shaping the chemical properties of GW.

In this study, ion ratio analysis [22,38] was conducted to further investigate the primary hydrogeochemical processes influencing the chemical composition of GW in the NJR. If the dissolution of halite is the sole source of Na^+ and Cl^- in groundwater, the Na^+/Cl^- ratio would equal 1, as the dissolution of halite releases equal amounts of Na^+ and Cl^- [39]. It can be seen from Figure 8a that the NJR GW samples are distributed on and off the line of $Na^+/Cl^- = 1$, and that four samples fall directly on the line, indicating that rock salt dissolution is a component of GW Na^+ and Cl^-, but is not the main source. The concentration of Na^+ and Cl^- in the GW is high, and 60% of the samples are above the $Na^+/Cl^- = 1$ line, indicating that there is an obvious evaporation and concentration process. In addition, the dissolution or cation exchange of silicate minerals may also be the reason for the presence of Na^+ in GW.

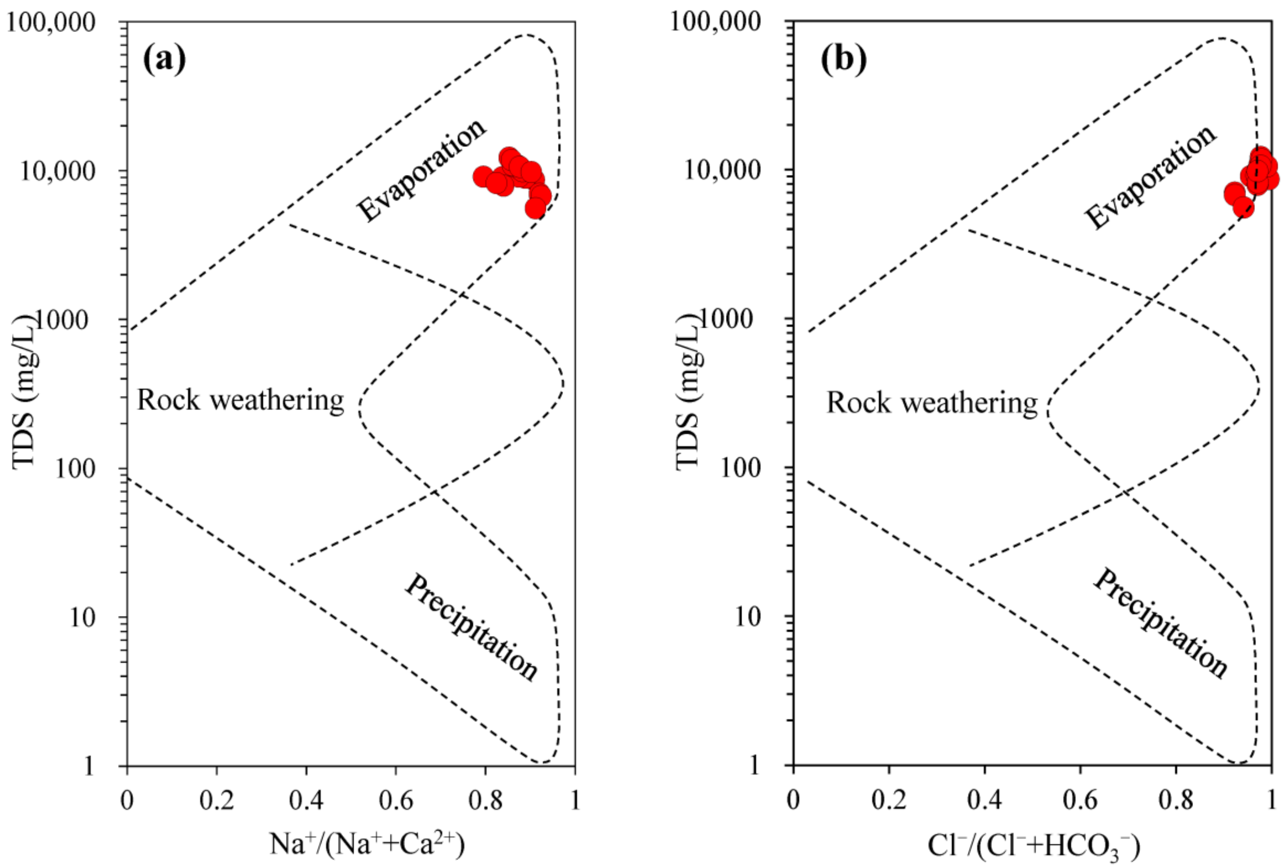

Figure 7. Gibbs diagram of deep GW samples in Northern Jinan. (**a**) Relationship between TDS and $Na^+/(Na^++Ca^{2+})$. (**b**) Relationship between TDS and $Cl^-/(Cl^-+HCO3^-)$.

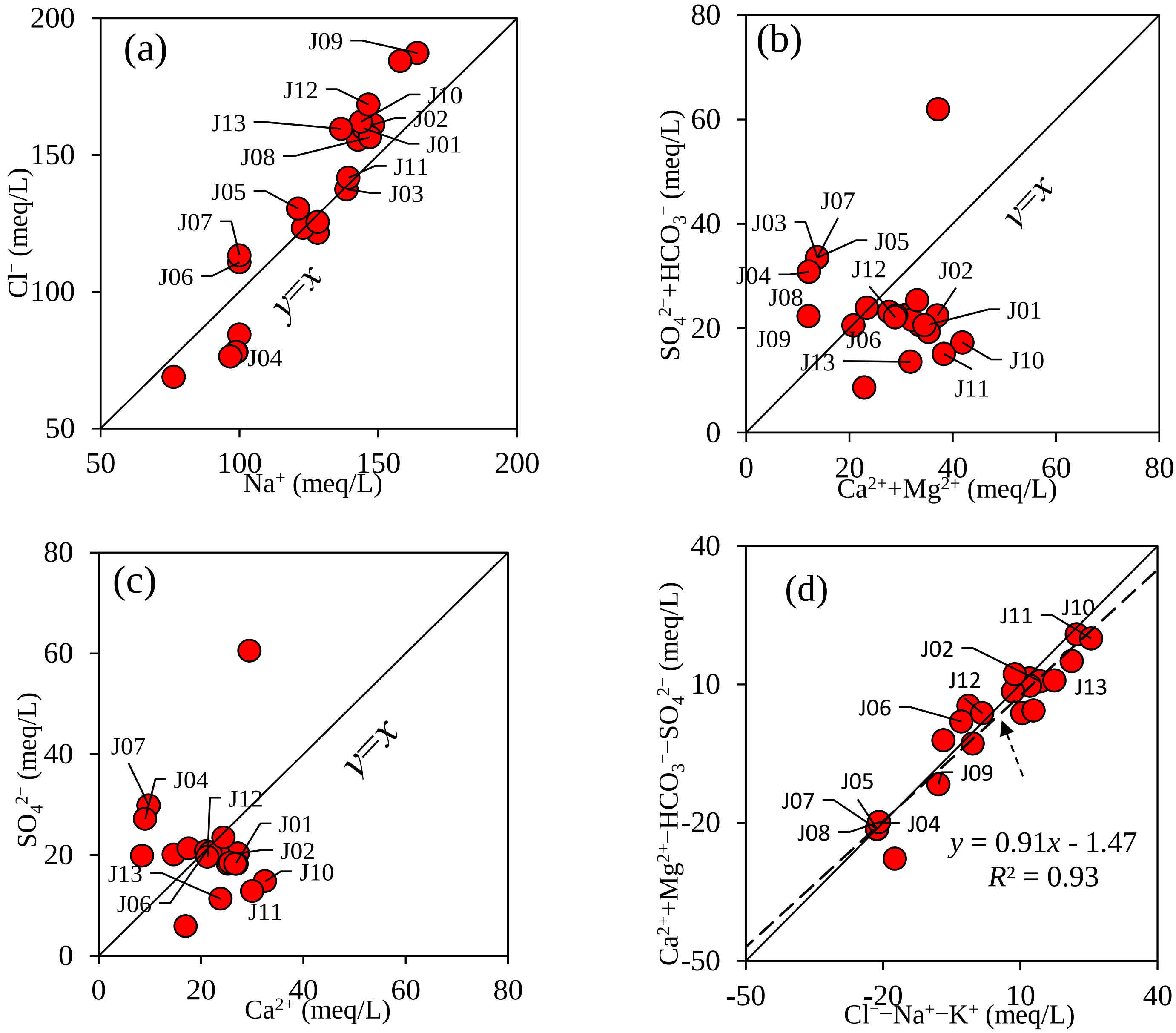

Figure 8. Binary scatter plot of major ion ratios in deep GW in northern Jinan. (**a**) Relationship between the ratios of Na^+ and Cl^-. (**b**) Relationship between the ratios of Ca^{2+}+Mg^{2+} and SO_4^{2-}+HCO_3^-. (**c**) Relationship between the ratios of Ca^{2+} and SO_4^{2-}. (**d**) Relationship between the ratios of Cl^--Na^+-K^+ and Ca^{2+}+Mg^{2+}-HCO_3^--SO_4^{2-}.

If the ratio of $[Ca^{2+} + Mg^{2+}]/[HCO_3^- + SO_4^{2-}]$ is greater than 1 in a water sample, it indicates that silicate weathering plays a significant role in influencing the water chemistry. Conversely, if the ratio is less than 1, it suggests that carbonate weathering is the main controlling factor [22,39]. It can be seen from Figure 8b that 70% of the GW samples of NJR are below the line of $[Ca^{2+} + Mg^{2+}]/[HCO_3^- + SO_4^{2-}] = 1$, indicating that the weathering of silicate rocks is the main controlling factor of the chemical composition of GW, and that the weathering of carbonate rocks also has a certain contribution. In addition, 80% of the GW samples deviate from the distribution of $[Ca^{2+}]/[HCO_3^-] = 1$ line (Figure 8c), and only two samples are close to it, indicating the presence of gypsum dissolution, but it is not the main source of Ca^{2+} and SO_4^{2-} in GW.

The relationship between $[Ca^{2+}+Mg^{2+}-HCO_3^--SO_4^{2-}]$ and $[Cl^--Na^+-K^+]$ is commonly used to identify the occurrence of cation exchange processes in the groundwater system [36,37]. When $[Ca^{2+}+Mg^{2+}-HCO_3^--SO_4^{2-}]/[Cl^--Na^+-K^+]$ equals 1, it signifies that cation exchange is an important hydrogeochemical process influencing the chemical characteristics of water. As depicted in Figure 8d, the GW samples in the NJR are distributed along the [Ca^{2+}+Mg^{2+}-HCO_3^--SO_4^{2-}]/[Cl^--Na^+-K^+] = 1 line, demonstrating a linear relationship between the data points, described by the equation y = 0.91x − 1.47 (R^2 = 0.93). This confirms that cation exchange is a significant factor impacting the chemical composition of deep GW in the NJR.

4.4.4. Mineral Dissolution Equilibrium

To determine the mineral dissolution and precipitation in GW, the equilibrium state of mineral phases was calculated using PHREEQC software [40], and the saturation index (SI) of the water samples was obtained. Figure 9 presents the statistical results of the SI values for relevant minerals. Overall, the SI values for carbonate minerals such as calcite, dolomite, and aragonite are all above 0, indicating that these minerals are in a supersaturated state and have a tendency to precipitate. On the other hand, the SI values for halite and gypsum are both below 0, indicating that these minerals are not yet in a state of saturation in the GW and will likely continue to dissolve along the water flow path. The SI values for quartz and chalcedony exhibit contrasting characteristics. The SI for quartz is consistently above 0, ranging from 0.16 to 0.28, while the SI for chalcedony is below 0, ranging from −0.18 to −0.06.

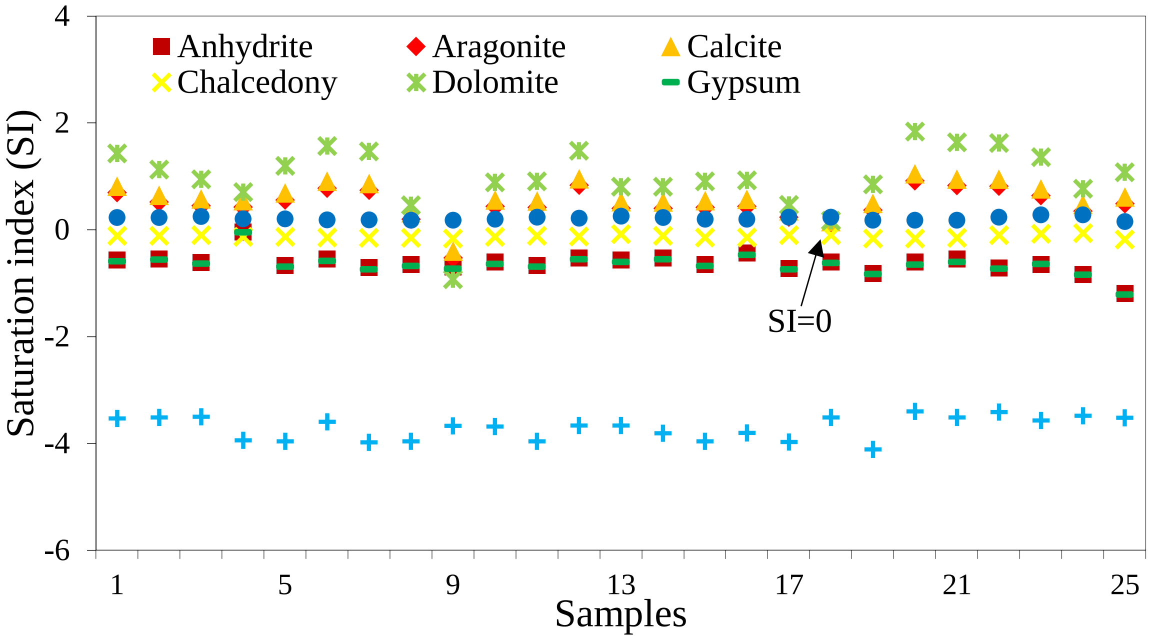

Figure 9. SI values for relevant minerals from deep GW in northern Jinan.

4.5. Genetic Analysis of Geothermal Field

The formation of GW is typically associated with various factors, including the cap layer (also known as the insulation layer), thermal storage capacity, heat source, and the source of thermal water recharge.

4.6. Geothermal Reservoir

The primary thermal reservoirs in the NJR consist of the Paleogene Dongying Formation and Guantao Formation. These thermal reservoirs are characterized by lithologies such as coarse sandstone, fine sandstone, and glutenite. The sediment grains exhibit medium roundness and average sorting, with argillaceous cementation. The glutenite shows poor diagenesis and loose properties. Notably, there are well-developed pores and fissures within the reservoir, resulting in a porosity range of 20 to 25%. This configuration provides ample space for efficient heat storage, creating a layered thermal reservoir with a pore-fracture structure. Overall, the thermal reservoir type found throughout the NJR is the Neogene Paleogene porous sandstone reservoir, with a particular focus on the Neogene Guantao Formation for geothermal development in the current stage.

4.7. Thermal Reservoir Overlying Strata

The stratum that sits above the thermal reservoir can be referred to as the thermal reservoir overlying strata. In the case of the Dongying Formation, the thermal reservoir overlying strata consists of the Guantao Formation, Minghuazhen Formation, and Quaternary deposits. These strata are primarily characterized by a soft layer composed of cohesive soil and sandy soil. They exhibit low density, considerable thickness, poor thermal conductivity, and significant thermal resistance. As a result, these strata naturally serve as effective thermal reservoir overlying layers.

4.8. Heat Source

The NJR primarily derives its heat source from the conduction heat flow of the upper mantle and the normal conduction heat flow of the deep crust. Additionally, the tectonic movement heat source and gravity compression heat source play significant roles and should not be disregarded. During the Mesozoic Yanshan Movement and Cenozoic Himalayan Movement, the region experienced the formation of multiple fault levels, accompanied by periods of magma intrusion. As a result, lava flows emerged along these faults, forming multilayer basic eruptive rocks. Over time, the area accumulated a substantial thickness of Cenozoic strata. Throughout geological history, the Cenozoic strata underwent compaction and diagenesis processes, releasing a substantial amount of heat energy. These various heat sources contribute to the overall heat stored within the thermal reservoir. The overlying thick layers of loose sediment act as thermal insulation, effectively preserving and retaining the heat within the reservoir.

4.9. Recharge Source of GW

The GW in the NJR is primarily replenished through lateral runoff from both nearby and distant mountainous areas during a long geological period following sediment deposition. While some sedimentary water and storage water remain trapped during the sedimentation process, the majority of the GW is recharged by runoff from the recharge areas. Based on regional paleogeographic conditions, these recharge areas could be located in the Taiyi mountains to the south or the Taihang mountains to the west. Once atmospheric precipitation infiltrates vertically, it undergoes a deep circulation within the aquifer along the horizontal direction. This recharge process is conducive to the replenishment of GW within the reservoir [41]. The conceptual model diagram illustrating the geothermal genesis for NJR is presented in Figure 10. This conceptual model of geothermal genesis highlights the contribution of lateral runoff from mountainous areas as the primary source of recharge for the GW in the NJR.

4.10. Conceptual Model of Geothermal Genesis

The convergence of atmospheric precipitation in the southern and western mountainous areas leads to the formation of surface currents. Over an extended geological timeframe, driven by the energy from head differences, this water migrates deep into the subsurface through fracture zones or the pores of rock formations. As it travels, it undergoes heating from the surrounding rocks and engages in complex water–rock reactions. The heated groundwater, influenced by the density differences caused by the temperature changes, contributes to natural convection. Along with the driving force from the head differences in the recharge area, this convection allows the groundwater to circulate slowly and alternately move (Figure 10). As it moves, the GW is stored within the pores and fissures, forming reservoirs within the geological formations. This process involves a combination of heat transfer, water–rock interactions, and groundwater movement, leading to the accumulation of GW in the area.

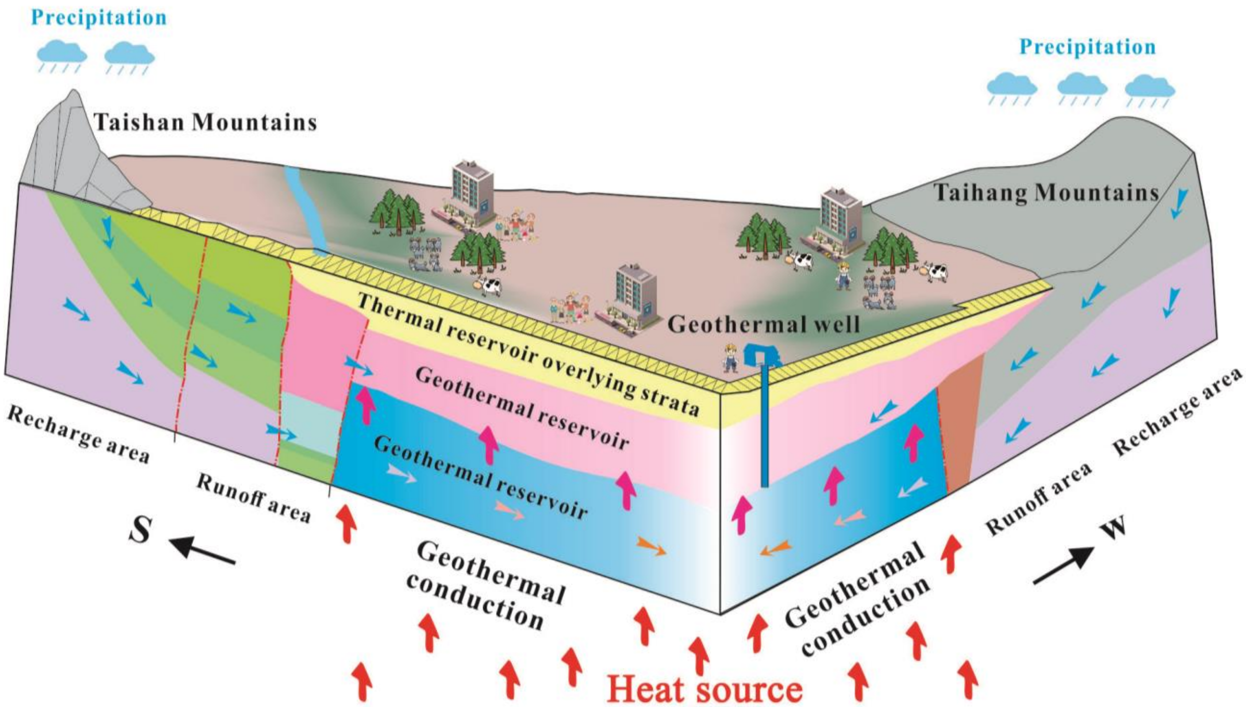

Figure 10. Conceptual model of geothermal field in the NJR.

5. Conclusions

Jinan possesses abundant geothermal resources, offering significant potential for development and utilization. Previous studies on geothermal resources in Jinan city have mainly focused on the southern section of the Qihe–Guangrao fault. Based on the geothermal geological conditions in the NJR, the chemical characteristics and formation mechanism of GW in the north of Jinan are analyzed by means of hydrochemistry and isotopes. Subsequently, a conceptual model of thermal storage is proposed. This provides a scientific basis and reference for the rational development and utilization of geothermal resources in Jinan city. The main findings and conclusions of this investigation are outlined below:

(1) The GW in the NJR exhibits relatively high salinity, with TDS content ranging from 5586.20 to 12,156.00 mg/L, and an average value of 9009.00 mg/L. The predominant ions in GW are Na^+ and Cl^-, with mean concentrations of 2829.73 mg/L and 4425.77 mg/L, respectively, resulting in the hydrochemical classification of GW as a Cl^-Na type. The cationic composition follows the order of $Na^+ > Ca^{2+} > Mg^{2+} > K^+$, while the anionic composition displays the sequence of $Cl^- > SO_4{}^{2-} > HCO_3{}^- > NO_3{}^-$.

(2) The δ^2H and δ^{18}O values of the GW ranged from −69.96 to −75.98 and −7.94 to −9.25, respectively, with mean values of −72.61 and −8.72, respectively. Analysis of the δ^2H and δ^{18}O isotopes suggests that the GW in the NJR originates from atmospheric precipitation that has undergone deep circulation and is mixed with older groundwater. Additionally, the composition of ^{3}H supports the notion that the GW is a result of water mixing. Furthermore, based on ^{14}C dating, it is inferred that the recharge of the GW likely occurred during the late Pleistocene period.

(3) The Na-K-Mg Giggenbach diagram reveals that all GWs in the NJR are partially equilibrated, indicating that the fluids and minerals have not achieved complete chemical equilibrium. There is significant variation in the temperature estimates obtained from different geothermometers. In this study, the quartz geothermometer is deemed more suitable for estimating the temperature of the geothermal reservoir, which ranges from 57.13 to 99.74 °C.

(4) In the long circulation process, GW undergoes continuous evaporation and leaching, resulting in its high salinity characteristics. The main sources of the chemical compo-

nents of the GW in the NJR are water–rock interactions, such as cation exchange, silicate weathering, carbonate weathering, and gypsum and halite dissolution. Calculations indicate that the SI of carbonate minerals is greater than 0, indicating oversaturation, while the SI values of halite and gypsum are both less than 0, indicating undersaturation.

(5) Based on the hydrogeological conditions, hydrochemistry, and isotope analysis of the NJR, a conceptual model of the geothermal field has been established. The GW is believed to originate from either Taiyi mountain in the south or Taihang mountain in the west, and thus experiences deep circulation and prolonged runoff time, contributing to the high salinity of the GW. These research findings provide valuable references and a foundation for the sustainable development and utilization of the regional geothermal resources in the area.

Supplementary Materials: The following supporting information can be downloaded at: https://www.mdpi.com/article/10.3390/en16227658/s1, Table S1: Data.

Author Contributions: Conceptualization, Z.G. and J.L.; methodology, M.H. and J.L.; formal analysis, M.H., Q.L., M.T. and Y.N.; writing—original draft preparation, M.H. and J.L.; writing—review and editing, Z.G. and J.L.; resources, Z.G. and M.H. All authors have read and agreed to the published version of the manuscript.

Funding: This research was funded by the Natural Science Foundation of Shandong Province (ZR2020MD109, ZR2021QD048).

Institutional Review Board Statement: Not applicable.

Informed Consent Statement: Not applicable.

Data Availability Statement: The data presented in this study are available in Supplementary Material Table S1.

Conflicts of Interest: The authors declare no conflict of interest.

References

1. Zhang, X.; Hu, Q. Development of geothermal resources in China: A Review. *J. Earth Sci.* **2018**, *29*, 452–467. [CrossRef]
2. Lund, J.W.; Toth, A.N. Direct utilization of geothermal energy 2020 worldwide review. *Geothermics* **2020**, *90*, 101915. [CrossRef]
3. Zhao, X.-G.; Wan, G. Current situation and prospect of China hebrew's geothermal resources. *Renew. Sustain. Energy Rev.* **2014**, *32*, 651–661. [CrossRef]
4. Li, X.; Qi, J.; Yi, L.; Xu, M.; Zhang, X.; Zhang, Q.; Tang, Y. Hydrochemical characteristics and evolution of geothermal waters in the eastern Himalayan syntaxis geothermal field, southern Tibet. *Geothermics* **2021**, *97*, 102233. [CrossRef]
5. Duan, R.; Li, P.; Wang, L.; He, X.; Zhang, L. Hydrochemical characteristics, hydrochemical processes and recharge sources of the geothermal systems in Lanzhou City, northwestern China. *Urban Clim.* **2022**, *43*, 101152. [CrossRef]
6. Ersoy, A.F.; Sönmez, S. Hydrogeochemical and isotopic characteristics of the Ilica geothermal system (Erzurum, Turkey). *Environ. Earth Sci.* **2014**, *72*, 4451–4462. [CrossRef]
7. Chenaker, H.; Houha, B.; Vincent, V. Hydrogeochemistry and geothermometry of thermal water from north-eastern Algeria. *Geothermics* **2018**, *75*, 137–145. [CrossRef]
8. Alçiçek, H.; Bülbül, A.; Brogi, A.; Liotta, D.; Ruggieri, G.; Capezzuoli, E.; Meccheri, M.; Yavuzer, I.; Alçiçek, M.C. Origin, evolution and geothermometry of the thermal waters in the Gölemezli Geothermal Field, Denizli Basin (SW Anatolia, Turkey). *J. Volcanol. Geotherm. Res.* **2018**, *349*, 1–30. [CrossRef]
9. Wang, X.; Lu, G.; Hu, B.X. Hydrogeochemical Characteristics and Geothermometry Applications of Thermal Waters in Coastal Xinzhou and Shenzao Geothermal Fields, Guangdong, China. *Geofluids* **2018**, *2018*, 8715080. [CrossRef]
10. Wang, X.; Zhou, X.; Zheng, Y.; Song, C.; Long, M.; Chen, T.; Ren, Z.; Yang, M.; Li, X.; Guo, J. Hydrochemical characteristics and mixing behavior of thermal springs along the Bijiang River in the Lanping basin of China. *Environ. Earth Sci.* **2017**, *76*, 487. [CrossRef]
11. Chiocchini, U.; Castaldi, F.; Barbieri, M.; Eulilli, V. A stratigraphic and geophysical approach to studying the deep-circulating groundwater and thermal springs, and their recharge areas, in Cimini Mountains–Viterbo area, central Italy. *Hydrogeol. J.* **2010**, *18*, 1319–1341. [CrossRef]
12. Belhai, M.; Fujimitsu, Y.; Bouchareb-Haouchine, F.Z.; Haouchine, A.; Nishijima, J. A hydrochemical study of the Hammam Righa geothermal waters in north-central Algeria. *Acta Geochim.* **2016**, *35*, 271–287. [CrossRef]
13. Başaran, C.; Gökgöz, A. Hydrochemical and isotopic properties of Heybeli geothermal area (Afyon, Turkey). *Arab. J. Geosci.* **2016**, *9*, 586. [CrossRef]

14. Wang, J.; Jin, M.; Jia, B.; Kang, F. Hydrochemical characteristics and geothermometry applications of thermal groundwater in northern Jinan, Shandong, China. *Geothermics* **2015**, *57*, 185–195. [CrossRef]
15. Sui, H.; Kang, F.; Li, C.; Han, J.; Xing, L. Relationship between north Ji'nan geothermal water and Ji'nan spring water revealed by hydrogeochemical characteristics. *Carsologica Sin.* **2017**, *36*, 49–58.
16. Kang, F.; Jin, M.; Qin, P. Sustainable yield of a karst aquifer system: A case study of Jinan springs in northern China. *Hydrogeol. J.* **2011**, *19*, 851–863. [CrossRef]
17. Wang, J.; Jin, M.; Lu, G.; Zhang, D.; Kang, F.; Jia, B. Investigation of discharge-area groundwaters for recharge source characterization on different scales: The case of Jinan in northern China. *Hydrogeol. J.* **2016**, *24*, 1723–1737. [CrossRef]
18. Li, C.; Wu, X.; Sun, B.; Sui, H.; Geng, F.; Qi, H.; Ma, X. Hydrochemical characteristics and formation mechanism of geothermal water in northern Ji'nan. *Earth Sci.* **2018**, *43*, 313–325.
19. Kang, F.; Sui, H.; Zheng, T. Heat accumulation and water enrichment mechanism of piedmont karstic geothermal reservoirs: A case study of northern Jinan. *Acta Geol. Sin.* **2020**, *94*, 1606–1624. [CrossRef]
20. Lei, T.; Liang, F.; Han, C.; Wang, Z.; Li, J.; Ma, Y.; Yao, H. Ambient Noise Tomography of Jinan: The Migration of Groundwater and the Formation of Geothermal Water. *Geol. J.* **2022**, *96*, 1716–1728. [CrossRef]
21. Piper, A.M. A graphic procedure in the geochemical interpretation of water-analyses. *Trans.-Am. Geophys. Union* **1944**, *25*, 914–923. [CrossRef]
22. Liu, J.; Peng, Y.; Li, C.; Gao, Z.; Chen, S. Characterization of the hydrochemistry of water resources of the Weibei Plain, Northern China, as well as an assessment of the risk of high groundwater nitrate levels to human health. *Environ. Pollut.* **2021**, *268*, 115947. [CrossRef]
23. Craig, H. Isotopic Variations in Meteoric Waters. *Science* **1961**, *133*, 1702–1703. [CrossRef]
24. Liu, J.; Song, X.; Yuan, G.; Sun, X.; Liu, X.; Wang, S. Characteristics of δ 18O in precipitation over Eastern Monsoon China and the water vapor sources. *Chin. Sci. Bull.* **2010**, *55*, 200–211. [CrossRef]
25. Mao, X.; Zhu, D.; Ndikubwimana, I.; He, Y.; Shi, Z. The mechanism of high-salinity thermal groundwater in Xinzhou geothermal field, South China: Insight from water chemistry and stable isotopes. *J. Hydrol.* **2021**, *593*, 125889. [CrossRef]
26. Fournier, R. Chemical geothermometers and mixing models for geothermal systems. *Geothermics* **1977**, *5*, 41–50. [CrossRef]
27. Clark, I.D.; Fritz, P. *Environmental Isotopes in Hydrology*; Lewis Publishers: Boca Raton, FL, USA, 1997. [CrossRef]
28. Arnórsson, S.; Gunnlaugsson, E.; Svavarsson, H. The chemistry of geothermal waters in Iceland. III. Chemical geothermometry in geothermal investigations. *Geochim. Cosmochim. Acta* **1983**, *47*, 567–577. [CrossRef]
29. Nieva, D.; Nieva, R. Developments in geothermal energy in Mexico—Part twelve. A cationic geothermometer for prospecting of geothermal resources. *Heat Recover. Syst. CHP* **1987**, *7*, 243–258. [CrossRef]
30. Giggenbach, W.; Gonfiantini, R.; Jangi, B.; Truesdell, A. Isotopic and chemical composition of parbati valley geothermal discharges, North-West Himalaya, India. *Geothermics* **1983**, *12*, 199–222. [CrossRef]
31. Fournier, R.; Truesdell, A. An empirical Na-K-MG-Ca geothermometer for natural waters. *Geochim. Cosmochim. Acta* **1973**, *37*, 1255–1275. [CrossRef]
32. Giggenbach, W.F. Geothermal solute equilibria. Derivation of Na-K-Mg-Ca geoindicators. *Geochim. Cosmochim. Acta* **1988**, *52*, 2749–2765. [CrossRef]
33. El Maghraby, M.M. Hydrogeochemical characterization of groundwater aquifer in Al-Madinah Al-Munawarah City, Saudi Arabia. *Arab. J. Geosci.* **2015**, *8*, 4191–4206. [CrossRef]
34. Aksever, F.; Büyükşahin, S. Erratum to: Assessment of variations in water quality using statistical techniques: A case study of Işıklı Lake, Çivril/Denizli, Turkey. *Arab. J. Geosci.* **2017**, *10*, 143. [CrossRef]
35. Han, D.; Liang, X.; Jin, M.; Currell, M.; Song, X.; Liu, C. Evaluation of groundwater hydrochemical characteristics and mixing behavior in the Daying and Qicun geothermal systems, Xinzhou Basin. *J. Volcanol. Geotherm. Res.* **2010**, *189*, 92–104. [CrossRef]
36. Gueroui, Y.; Maoui, A.; Touati, H.; Guettaf, M.; Bousbia, A. Hydrogeochemical and environmental isotopes study of the northeastern Algerian thermal waters. *Environ. Earth Sci.* **2018**, *77*, 747. [CrossRef]
37. Gibbs, R.J. Mechanisms Controlling World Water Chemistry. *Science* **1970**, *170*, 1088–1090. [CrossRef]
38. Zhao, Q.; Luo, Z.; Du, J.; Wang, L.; Li, Z.; Wang, X. Hydrogeochemical characteristics and genesis of geothermal water in Xiaoyangkou, Nantong. *China Environ. Earth Sci.* **2023**, *82*, 456. [CrossRef]
39. Liu, J.; Gao, Z.; Wang, Z.; Xu, X.; Su, Q.; Wang, S.; Qu, W.; Xing, T. Hydrogeochemical processes and suitability assessment of groundwater in the Jiaodong Peninsula, China. *Environ. Monit. Assess.* **2020**, *192*, 384. [CrossRef]
40. Liu, J.; Wang, M.; Gao, Z.; Chen, Q.; Wu, G.; Li, F. Hydrochemical characteristics and water quality assessment of groundwater in the Yishu River basin. *Acta Geophys.* **2020**, *68*, 877–889. [CrossRef]
41. Dallai, L.; Magro, G.; Petrucci, E.; Ruggieri, G. Stable isotope and noble gas isotope compositions of inclusion fluids from Larderello geothermal field (Italy): Constraints to fluid origin and mixing processes. *J. Volcanol. Geotherm. Res.* **2005**, *148*, 152–164. [CrossRef]